J Neuropathol Exp Neurol
Vol. 79, No. 7, July 2020, pp. 800–808
doi: 10.1093/jnen/nlaa035

ORIGINAL ARTICLE

Activation of CaMKII and GluR1 by the PSD-95-GluN2B Coupling-Dependent Phosphorylation of GluN2B in the Spinal Cord in a Rat Model of Type-2 Diabetic Neuropathic Pain

Ya-Bing Zhu, MD, Gai-Li Jia, MD, Jun-Wu Wang, BD, Xiu-Ying Ye, BD, Jia-Hui Lu, MD, Jia-Li Chen, MD, Mao-Biao Zhang, MD, Ci-Shan Xie, BD, Yu-Jing Shen, BD, Yuan-Xiang Tao, PhD, MD, Jun Li, PhD, and Hong Cao, MD

Abstract

The mechanisms underlying type-2 diabetic neuropathic pain (DNP) are unclear. This study investigates the coupling of postsynaptic density-95 (PSD-95) to N-methyl-D-aspartate receptor subunit 2B (GluN2B), and the subsequent phosphorylation of GluN2B (Tyr1472-GluN2B) in the spinal cord in a rat model of type-2 DNP. Expression levels of PSD-95, Tyr1472-GluN2B, Ca^{2+}/calmodulin-dependent protein kinase II (CaMKII) and its phosphorylated counterpart (Thr286-CaMKII), and α-amino-3-hydroxy-5-methyl-4-soxazole propionic acid receptor subtype 1 (GluR1) and its phosphorylated counterpart (Ser831-GluR1) were significantly increased versus controls in the spinal cord of type-2 DNP rats whereas the expression of total spinal GluN2B did not change. The intrathecal injection of Ro25-6981 (a specific antagonist of GluN2B) or Tat-NR2B9c (a mimetic peptide disrupting the interaction between PSD-95 and GluN2B) induced an antihyperalgesic effect and blocked the increased expression of Tyr1472-GluN2B, CaMKII, GluR1, Thr286-CaMKII, and Ser831-GluR1 in the spinal cords; the increase in spinal cord PSD-95 was not affected. These findings indicate that the PSD-95-GluN2B interaction may increase phosphorylation of GluN2B, and subsequently induce the expression of phosphorylation of CaMKII and GluR1 in the spinal cord of type-2 DNP rats. Targeting the interaction of PSD-95 with GluN2B may provide a new therapeutic strategy for type-2 DNP.

Key Words: Diabetes, GluN2B, Neuropathic pain, PSD-95, Spinal cord.

INTRODUCTION

The incidence of diabetes mellitus (DM) has dramatically increased during the past 2–3 decades (1), and type-2 DM (T2DM) accounts for ∼90% of cases (2). One of the most common complications of DM is diabetic neuropathy (DN), which occurs in ∼50% of DM patients (3); more than 30% of these patients suffer from diabetic neuropathic pain (DNP) (4–6). DNP has been characterized by spontaneous pain, hyperalgesia, and allodynia (7), and is difficult to treat (8). Although some of the potential mechanisms underlying DNP have been identified (7), the exact pathophysiological mechanisms remain elusive. Accumulating evidence suggests that spinal cord central sensitization may play significant roles in the development of neuropathic pain, as well as DNP (9). N-methyl-D-aspartate receptor (NMDAR), an ionotropic glutamate receptor, is activated in the spinal cord dorsal horn under conditions of neuropathic pain (10–12), and blocking spinal NMDARs attenuated the neuropathic pain (13). Preclinical evidence has suggested that NMDARs are involved in the dorsal horn central sensitization following neurological damage. However, NMDAR antagonists have caused severe side effects, limiting their application in clinical settings (14, 15). Recent evidence has revealed that targeting the NMDAR NR2B subunit would likely reduce its side effects (16). Furthermore, the expression of spinal NMDAR subunit receptor 2B (GluN2B) is elevated in streptozotocin (STZ)-induced type-1 DNP (17). Ro25-6981 is a GluN2B-selective antagonist, and the intrathecal administration of Ro25-6981 can reduce tactile allodynia in rats with pre-DNP (18). However, the role of GluN2B in type-2 DNP remains unclear. Postsynaptic density protein-95 (PSD-95), which is an NMDAR-anchoring protein, contains 3 PSD-95/discs large protein/ZO1 (PDZ) domains. The second PDZ domain constitutes the signaling complexes that modulate the efficacy of NMDAR-mediated

From the Department of Anesthesiology, The Second Affiliated Hospital and Yuying Children's Hospital of Wenzhou Medical University, Pain Medicine Institute of Wenzhou Medical University, Zhejiang, China (YBZ, GLJ, JWW, XYY, JHL, JLC, MBZ, CSX, YJS, JL, HC); Department of Anesthesiology, Shanghai General Hospital, Shanghai Jiao Tong University School of Medicine, Shanghai, China (YBZ); and Department of Anesthesiology, New Jersey Medical School, Rutgers, The State University of New Jersey, Newark, New Jersey (YXT).

Send correspondence to: Hong Cao, MD, Department of Anesthesiology, The Second Affiliated Hospital and Yuying Children's Hospital of Wenzhou Medical University, Pain Medicine Institute of Wenzhou Medical University, No 109, West College Road, Lucheng District, Zhejiang 325027, China. E-mail: caohong1955@21cn.com

This study was supported by National Natural Science Foundation of China (Project No. 81771487) and Zhejiang Provincial Natural Science Foundation of China (Project No. LY17H070006).

The authors have no duality or conflicts of interest to declare.

Supplementary Data can be found at academic.oup.com/jnen.

neurotransmission (19). Although the expression of PSD-95 is significantly increased in neuropathic pain models, the mutation or suppression of PSD-95 remains therapeutically impractical due to severe side effects (10). Previous studies have shown that the interaction between PSD-95 and GluN2B can trigger the phosphorylation of GluN2B and result in the enhancement of synaptic plasticity and pain hypersensitivity (20–22). Disrupting the PSD-95-GluN2B interaction through the intrathecal injection of the mimetic peptide Tat-NR2B9c can reverse formalin-induced pain behavior but not alter calcium influx through NMDARs (20). Therefore, interfering with the PSD-95-GluN2B interaction may minimize NMDAR-induced side effects. Given that the phosphorylation of GluN2B at Tyr1472 (Tyr1472-GluN2B) is essential for the maintenance of neuropathic pain (23), we initially determined whether the level of spinal Tyr1472-GluN2B increased in the spinal cord of type-2 DNP rats, and whether intrathecal Ro25-6981 or perturbing the interaction of PSD-95-GluN2B could limit the increase of Tyr1472-GluN2B, or have an antinociceptive effect on type-2 DNP.

After the activation of the NMDAR receptor, the NMDAR channels become permeable to calcium ions (Ca^{2+}) leading to the autophosphorylation of Ca2+/calmodulin-dependent protein kinase II (CaMKII) on Thr286 (Thr286-CaMKII) (24). CaMKII can bind to GluN2B subunits in the PSD, which promotes the phosphorylation of α-amino-3-hydroxy-5-methyl-4-soxazole propionic acid receptors (AMPAR) subunit 1 (GluR1) on Ser831 (Ser831-GluR1), thereby enhancing the single-channel conductance of synaptic AMPAR (25). The activation of CaMKII occurs downstream of Tyr1472-GluN2B and this resulted in neuropathic pain after spared nerve injury, while the inhibition of the activation of CaMKII by KN93, a CaMKII inhibitor, reduced the phosphorylation of GluR1, and relieved the pain behavior (26). The role of CaMKII and GluR1 in type-2 DNP remains unclear, however. Therefore, we examined the expression and phosphorylation of CaMKII and GluR1 in the spinal cord in a rat model of type-2 DNP.

MATERIALS AND METHODS

Animals

Six-week-old male Sprague Dawley rats (Approval No. wydw2017-005, SCXK [Zhe-jiang] 2005-0019), weighing 130–150 g, were housed in a temperature-controlled room (23°C–25°C) with a 12-/12-hour dark/light cycle, and food and water ad libitum. All experimental procedures were performed in accordance with the Animal Use Committee of Wenzhou Medical University.

Type-2 DNP Model and Experimental Grouping

The type-2 DNP model was established as previously described (27). Rats were randomly assigned into 2 groups (groups C and D). In group C (n = 6), rats were fed with normal diet as controls. In group D (n = 60), rats were fed with high-sugar and high-fat diet, as previously described (27), which included 67% normal diet plus 10% lard, 20% sucrose, 2% cholesterol, and 1% sodium cholate, in order to induce insulin resistance (Supplementary Data Fig. S1). The behavioral responses (mechanical withdrawal threshold, [MWT]; thermal withdrawal latency, [TWL]), fasting blood glucose and insulin level were first measured as the baseline levels. After 8 weeks of high-sugar and high-fat diet, the fasting blood glucose and insulin levels were measured again, and the insulin sensitivity index was calculated. Rats in group D were then intraperitoneally injected with STZ (35 mg/kg, Sigma Aldrich, St Louis, MO), whereas rats in group C were intraperitoneally injected with the same dose of citrate buffer. After 3 days, the fasting blood glucose in group D was measured again. Rats with a fasting blood glucose of ≥16.7 mmol/L in the tail vein were diagnosed as type-2 diabetic rats. A previous study suggested that in diabetes model rats, STZ-induced mechanical allodynia and thermal hyperalgesia usual occur after 1 week and reach the peak level after 2 weeks (28). Therefore, the MWT and TWL of these rats were measured again after 2 weeks. Rats with both MWT and TWL values of ≤85% of the baseline level were regarded as type-2 DNP rats (29, 30). Rats diagnosed as type-2 DNP were randomly divided into 4 groups: no injection (n = 18); injection with Ro25-6981 (group Ro, n = 6); injection with Tat-NR2B9c (group Ta, n = 6); and injection with vehicle (group SC, n = 6). Type-2 diabetic rats with both MWT and TWL values of >85% of the baseline values were assigned as type-2 diabetic painless rats (group DA, n = 6). Since approximately 80% of type-2 diabetic rats developed type-2 DNP (27), the investigators had to prepare more rats at the beginning to meet the requirements for the minimum number of animals per group (at least 6 rats/group).

Determination of Insulin by Enzyme Linked Immunosorbent Assay and Calculation of the Insulin Sensitivity Index

In total,1 mL of tail vein blood was collected from rats after fasting for 12 hours. After the blood samples were centrifuged, the supernatants were collected to measure the insulin level using the enzyme linked immunosorbent assay method (kits were purchased from Haixi Tang Biotechnology Co., Ltd., Shanghai, China). The insulin sensitivity index was calculated based on the following formula: insulin sensitivity index = 1/(fasting glucose × fasting insulin). The natural logarithm used to calculate these data was not normally distributed (31).

Behavioral Tests

Behavioral tests were carried out before STZ injection and on days 14, 17, 21, and 28 after STZ injection. All measurements were carried out at 8–11 AM in a quiet environment, with the room temperature maintained at 24°C ± 1°C. The experimenters were blinded to the grouping.

Mechanical Withdrawal Threshold

Rats were placed into a Plexiglas chamber (22 × 22 × 22 cm) and were allowed to adapt to the chamber for 30 minutes. The MWT test was performed by vertically stimulating the surface of the rear toes using the IITC 2390 series electronic von Frey tactile pain measurement instrument

(Woodland Hills, CA), with an interval of 10 seconds and a single-stimulus hold of ≤1 second. During the test, the intensity of the stimulus was recorded when the rat paw was withdrawn, with or without licking. The MWT test was repeated 5 times with an interval of 5 minutes. The average intensity of the MWT values was calculated, as previously reported (32).

Thermal Withdrawal Latency

An IITC 336 plantar/tail flick analgesia meter (Woodland Hills, CA) was used to measure the TWL. Rats were placed in individual transparent plexiglass compartments (20 × 15 × 30 cm) on a 3-mm glass plate and thermal radiation was exposed directly to the toe. The time from the initiation of irradiation to toe lift was recorded as the TWL. The stimulation was repeated 5 times with an interval of 5 minutes. The mean value was regarded as TWL (33).

Intrathecal Catheter

Under deep anesthesia with chloral hydrate (0.3 g/kg), a PE-10 silastic tubing (Ningbo Science and Technology Park, The Software Technology Co., Ltd, Zheijiang, China) was intrathecally inserted between the L4 and L5 vertebrae and was advanced 2 cm into the lumbar enlargement of the spinal cord. The external end of the intrathecal catheter was tunneled under the skin to the neck area. After the surgery, the animals were given penicillin for 3 days to prevent infection and given 5–6 days for recovery. In order to verify the location of the catheter, 10 μL of 2% lidocaine was given through the catheter. A limb paralysis response without neurological deficits indicated the correct location of the catheter (34).

Intervention of Drugs

After successfully implanting the intrathecal catheter, the vehicle (i.e. normal saline), 200 μg/10 μL of Ro25-6981 (Sigma Aldrich, Cat. No. R7150) and 150 ng/10 μL of Tat-NR2B9c (MedChem Express, Monmouth Junction, NJ, Cat. No. 500992-11-0) were injected for 14 consecutive days, respectively. The behavioral tests were carried out on days 3, 7, and 14 after the injection.

Western Blot Analysis

After the behavior tests, rats were euthanized, and the spinal lumbar enlargement segments were collected and rapidly stored in liquid nitrogen. The tissues were homogenized in lysis buffer (1:10 wt/vol) comprised of 0.32 M of sucrose, 2 mM of EDTA, 10 mM of sodium phosphate, 2 mM of dithiothreitol, 1 mM of Phenylmethylsulfonyl fluoride, Protease and Phosphatase inhibitors (Sigma Aldrich), and 20 mM of Tris-HCl. After centrifugation at 12 000 rpm at 4°C, the supernatant was collected as the cytosolic proteins. The protein concentration was measured by bicinchoninic acid assay. The protein samples (30 μg/sample) were heated at 99°C for 5 minutes and loaded onto a 12% sodium dodecyl sulfate polyacrylamide gel electrophoresis (SDS-PAGE) gel. These proteins were then transferred onto polyvinylidene fluoride (PVDF) membranes using an electrophoretic transfer film instrument (Bio-Rad, Hercules, CA). Afterwards, these membranes were blocked with 10% nonfat milk dissolved in Tris-buffered saline-Tween (TBST) solution for 2 hours at room temperature before the membranes were incubated with antibodies. The primary antibodies were as follows: polyclonal rabbit anti-tGluN2B (1:1000, Cell Signaling Technology, Danvers, MA; Cat. No. 14544S), polyclonal rabbit Tyr1472-GluN2B (1:1000, Cell Signaling Technology; Cat. No. 4208S, RRID: AB-1549657), polyclonal rabbit anti-GluR1 (1:500, Abcam, Cambridge, UK; Cat. No. ab31232), monoclonal mouse anti-PSD-95 (1:500, Abcam; Cat. No. ab99009, RRID: AB-10676078), monoclonal mouse anti-p-CaMKII (Thr286-CaMKII; 1:500, Abcam, Cat. No. ab171095), monoclonal rabbit anti-CaMKII (1:1000, Abcam; Cat. No. ab52476), and monoclonal rabbit anti-GluR1 (Ser831-GluR1; 1:1000; Abcam, Cat. No. ab109464, RRID: AB-10862154), or rabbit anti-β-actin (AP0060). These were incubated at 4°C overnight. After the membranes were extensively washed with TBST at room temperature, the membranes were incubated with goat antirabbit immunoglobulin G (IgG) (1:3000, Zymed, Waltham, MA; Cat. No. A32735, RRID: AB-2633284) or goat antimouse IgG (1:3000, Zymed; Cat. No. A32729, RRID: AB-2633278) in 5% nonfat milk dissolved in TBST for 2 hours. The signals were detected by enhanced chemiluminescence. The density of the specific bands was analyzed using Alpha Ease FC software, and the expression levels of these proteins were normalized to β-actin.

Coimmunoprecipitation

In total, 5 μg of mouse monoclonal anti-PSD-95 antibody (1:100, Abcam; Cat. No. ab99009) were incubated with the homogenized fraction from the spinal cord dorsal horn overnight at 4°C. The protein A/G plus agarose (Santa Cruz Biotechnology, Santa Cruz, CA; Cat. No. sc2003, RRID: AB-10201400) was added into the mixture and incubated at 4°C for 2 hours. After this incubation, the agarose beads were washed with the immunoprecipitation buffer (1% Triton X-100, 50 mM of Tris-Cl, pH 7.4, 5 mM of ethylenediaminetetraacetic acid, and 0.02% sodium azide), with or without 300 mM of NaCl, 3 times. The binding proteins were separated using SDS-PAGE, electrophoretically transferred onto PVDF membranes, and detected using monoclonal goat anti-PSD-95 (1:500, Abcam; Cat. No. ab99009) and rabbit anti-tGluN2B (1:1000, Cell Signaling Technology, Cat. No. 14544S).

Statistical Analysis

No statistical methods were used to predetermine the sample sizes for these studies, but the present sample sizes were the same as those used in a previous study (27). The data are presented as mean ± SD. Box plots were used to determine the outliers, and these were excluded. Shapiro-Wilk tests were used to determine whether the data conformed to the normal distribution. The data were statistically analyzed using 1-

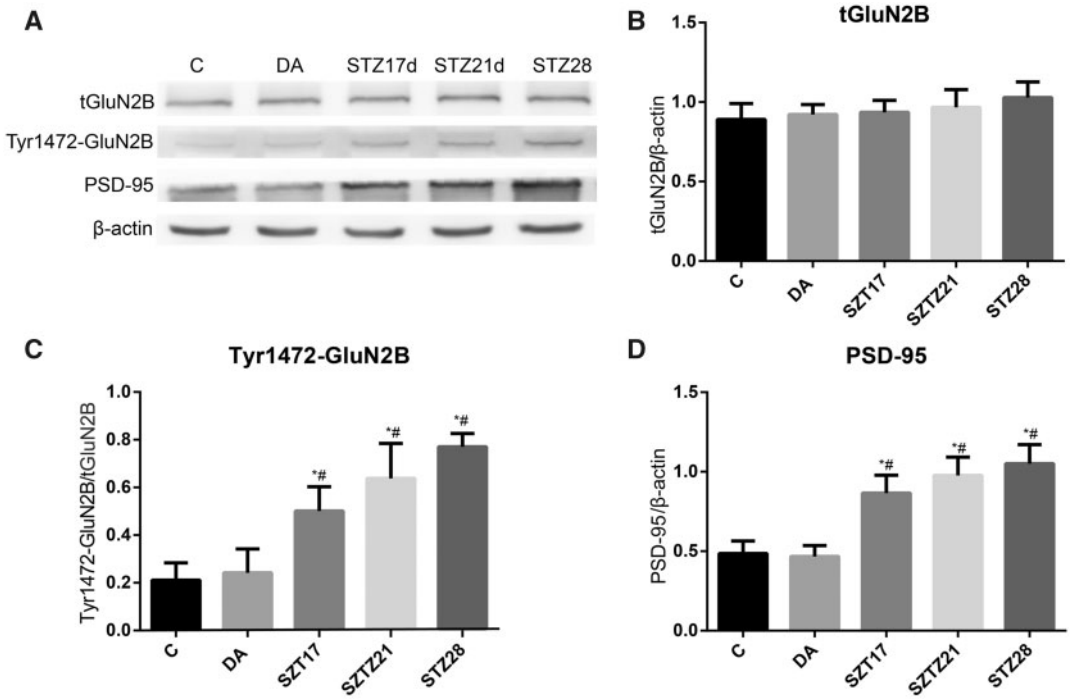

FIGURE 1. Expression of tGluN2B and PSD-95 protein, and the GluN2B phosphorylation at Tyr1472 in the spinal cord in the different groups. **(A)** Western blot analysis for the tGluN2B, Tyr1472-GluN2B, and PSD-95 protein in the spinal cord in the different groups at different time points. **(B–D)** Three histograms summarize the integrated density values of tGluN2B, Tyr1472-GluN2B, and PSD-95, respectively (normalized to the β-actin level), in the 5 groups. Groups C and DA: n = 6 rats/group, Group DNP of STZ 17, 21, and 28: n = 6 rats/each time point. *$p < 0.05$ versus group C, #$p < 0.05$ versus group DA.

or 2-way analysis of variance (ANOVA), or paired or unpaired Student *t*-test. When the ANOVA exhibited a significant difference, pairwise comparisons between means were tested using the post hoc Tukey's method. Data were analyzed using SPSS 16.0 (SPSS Inc., Chicago, IL). A p value of < 0.05 was considered significant.

RESULTS

Validation of Type-2 DNP

A rat model of type-2 DNP was first established by providing a high-sugar and high-fat diet to create a state of insulin resistance, in combination with the single intraperitoneal administration of STZ. After rats were fed with high-sugar and high-fat diet for 8 weeks, the body weights became significantly higher than control rats fed with a normal diet (Supplementary Data Fig. S2, $p < 0.05$). The levels of blood glucose in group D were 5.76 ± 0.97 mmol/L at the eighth week, which, as expected, was higher than those in group C (2.95 ± 0.46 mmol/L) (Supplementary Data Table S1, $p < 0.05$). Furthermore, the levels of insulin in group D (40.07 ± 7.64 mIU/L) were markedly elevated versus those in group C (16.01 ± 2.44 mIU/L). Consistently, the insulin sensitivity indices in group D (-5.41 ± 0.25) were significantly decreased when compared with those in group C (-3.85 ± 0.56; Supplementary Data Table S1, $p < 0.05$). In addition, on the third day after STZ injection, the levels of blood glucose in diabetic rats (29.83 ± 3.10 mmol/L) were dramatically increased versus those in group C (Supplementary Data Table S1, $p < 0.05$). Given that the average levels in diabetic rats were >16.7 mmol/L (24), the experimental rats used in this study completely developed the model of type-2 diabetes. Finally, rats in group DNP exhibited significantly decreased values of both MWT and TWL from the 14th to the 28th days after STZ injection compared with those in group C or DA (Supplementary Data Fig. S2, $p < 0.05$). These data indicate that the neuropathic pain induced by type-2 diabetes was successfully established.

Increased Expression of PSD-95 and Tyr1472-GluN2B in the Spinal Cord of Type-2 DNP Rats

The levels of total GluN2B protein (tGluN2B) in the spinal cord between groups DNP and group C were not statistically significant (Fig. 1A, B), but the level of phosphorylation of GluN2B at Tyr1472 (Tyr1472-GluN2B) in group DNP was significantly elevated. Therefore, the ratios of Tyr1472-GluN2B/tGluN2B increased on the 17th (0.50 ± 0.04), 21st (0.64 ± 0.06), and 28th (0.77 ± 0.02) days after STZ injection, when compared with group C (Fig. 1C; 0.21 ± 0.03, $p < 0.05$) and group DA (Fig. 1C; 0.24 ± 0.04, $p < 0.05$). Furthermore, the expression of PSD-95 in group DNP also increased on the 17th (0.87 ± 0.05), 21st (0.98 ± 0.05), and 28th (1.05 ± 0.05) days (Fig. 1D). These findings indicate that PSD-95 and

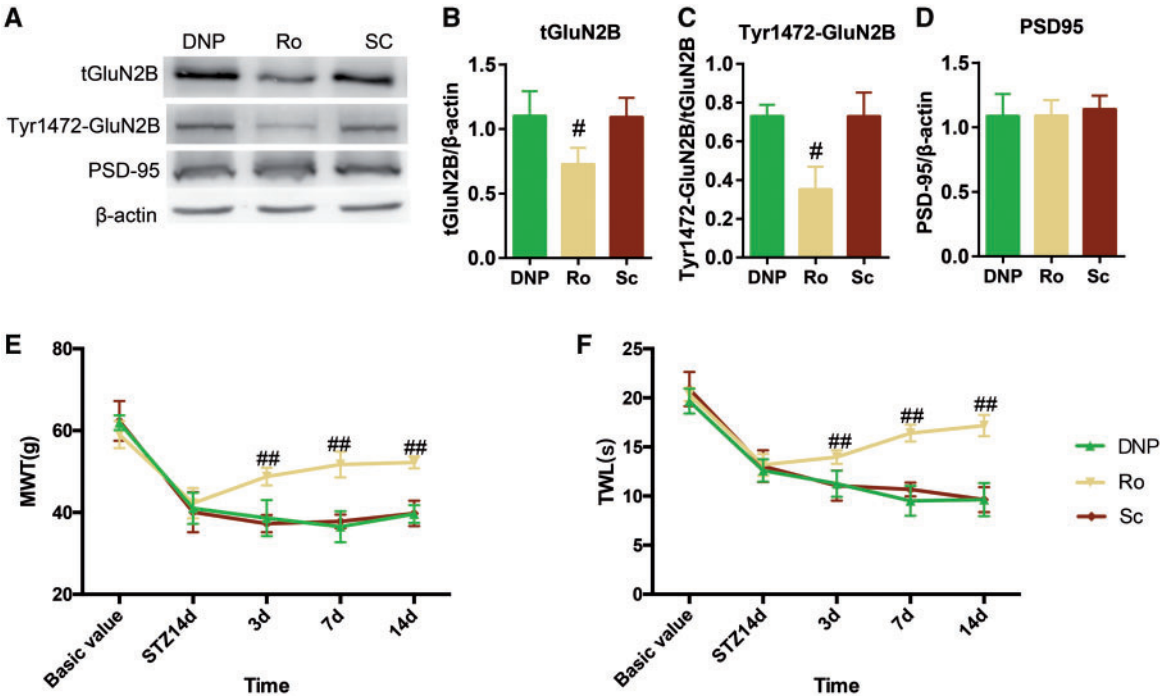

FIGURE 2. Ro25-6981 alleviated pain behavior and reduced the expression of tGluN2B and GluN2B phosphorylation at Tyr1472 in type-2 DNP rats. **(A)** Western blot results of the tGluN2B, Tyr1472-GluN2B, and PSD-95 protein in the different groups. **(B–D)** The histogram summarizes the integrated density values of tGluN2B, Tyr1472-GluN2B/tGluN2B, and PSD-95, respectively, in the 3 groups. **(E, F)** The changes in mechanical withdrawal threshold **(**MWT; **E)** and thermal withdrawal latency **(**TWL; **F)**. Group DNP: diabetic rats with neuropathic pain, Group Ro: DNP rats + Ro25-6981, Group Sc: DNP rats + saline (n = 6 rats/each group). $^{\#\#}p < 0.05$ versus group DNP.

Tyr1472-GluN2B in the spinal cord may participate in the process of type-2 DNP.

Intrathecal Ro25-6981 Blocked the Phosphorylation of GluN2B at Tyr1472 in the Spinal Cord and Alleviated Pain Hypersensitivity in Type-2 DNP

The role of GluN2B in type-2 DNP was further investigated through the intrathecal injection of Ro25-6981, which is a specific GluN2B antagonist. The drug was administered for 3, 7 and 14 consecutive days starting from the 14th day after STZ injection. Behavioral tests were carried out within 2 hours after intrathecal Ro25-6981 injection. The administration of Ro25-6981 significantly blocked the increase in tGluN2B and Tyr1472-GluN2B expression (Fig. 2A, B; DNP: 1.13 ± 0.08, Ro: 0.73 ± 0.05, $p < 0.05$). The ratio of Tyr1472-GluN2B/tGluN2B also decreased (Fig. 2C; DNP: 0.73 ± 0.02, Ro: 0.35 ± 0.05, $p < 0.05$). Furthermore, Ro25-6981 attenuated the reduction in MWT and TWL in type-2 DNP rats, when compared with DNP rats (Fig. 2E, F; $p < 0.05$). However, the intrathecal administration of Ro25-6981 had no effect on the expression of PSD-95 (DNP: 1.09 ± 0.17, Ro: 1.09 ± 0.12; $p > 0.05$) in type-2 DNP. These present results indicate that the intrathecal administration of Ro25-6981 alleviated the pain hypersensitivities possibly through the inhibition of the phosphorylation of GluN2B at Tyr1472 in type-2 DNP rats. This result suggests that Tyr1472-GluN2B may play an important role in the development of type-2 DNP.

Interference of Spinal PSD-95-GluN2B Coupling Blocked the Increase in Spinal Cord GluN2B Phosphorylation at Tyr1472 and Pain Hypersensitivity in Type-2 DNP Rats

To investigate the role of spinal PSD-95-GluN2B coupling in type-2 DNP, the effect of Tat-NR2B9c, which is a mimetic peptide that could perturb the interaction of PSD-95 with GluN2B, on GluN2B protein phosphorylation, as well as the PSD-95 protein expression and pain behavior, were examined. Coimmunoprecipitation results revealed that the coupling of PSD-95 and GluN2B in DNP rats treated with Tat-NR2B9c were significantly decreased when compared with DNP rats without the treatment (Fig. 3A, B), indicating that Tat-NR2B9c could perturb the interaction between PSD-95 and GluN2B. The intrathecal administration of Tat-NR2B9c blocked the phosphorylation of GluN2B at Tyr1472, which was demonstrated by the decrease in the ratio of Tyr1472-GluN2B/tGluN2B (Fig. 3C, D; DNP: 0.78 ± 0.04, Ta: 0.49 ± 0.02, $p < 0.05$), without affecting the expression of PSD-95 (DNP: 1.02 ± 0.13, Ta: 1.01 ± 0.09, $p > 0.05$) and tGluN2B (DNP: 1.04 ± 0.05, Ta: 1.05 ± 0.07, $p > 0.05$) in the spinal cord dorsal horn of type-2 DNP rats. The reduction in both MWT and TWL was time-dependently rescued in type-2 DNP after the intrathecal administration of Tat-NR2B9c (Fig. 3F, G; $p < 0.05$). These data suggest that the blocked interaction between the PSD-95 and GluN2B coupling attenuated the pain hypersensitivities by decreasing Tyr1472-GluN2B. The coupling of PSD-95 and

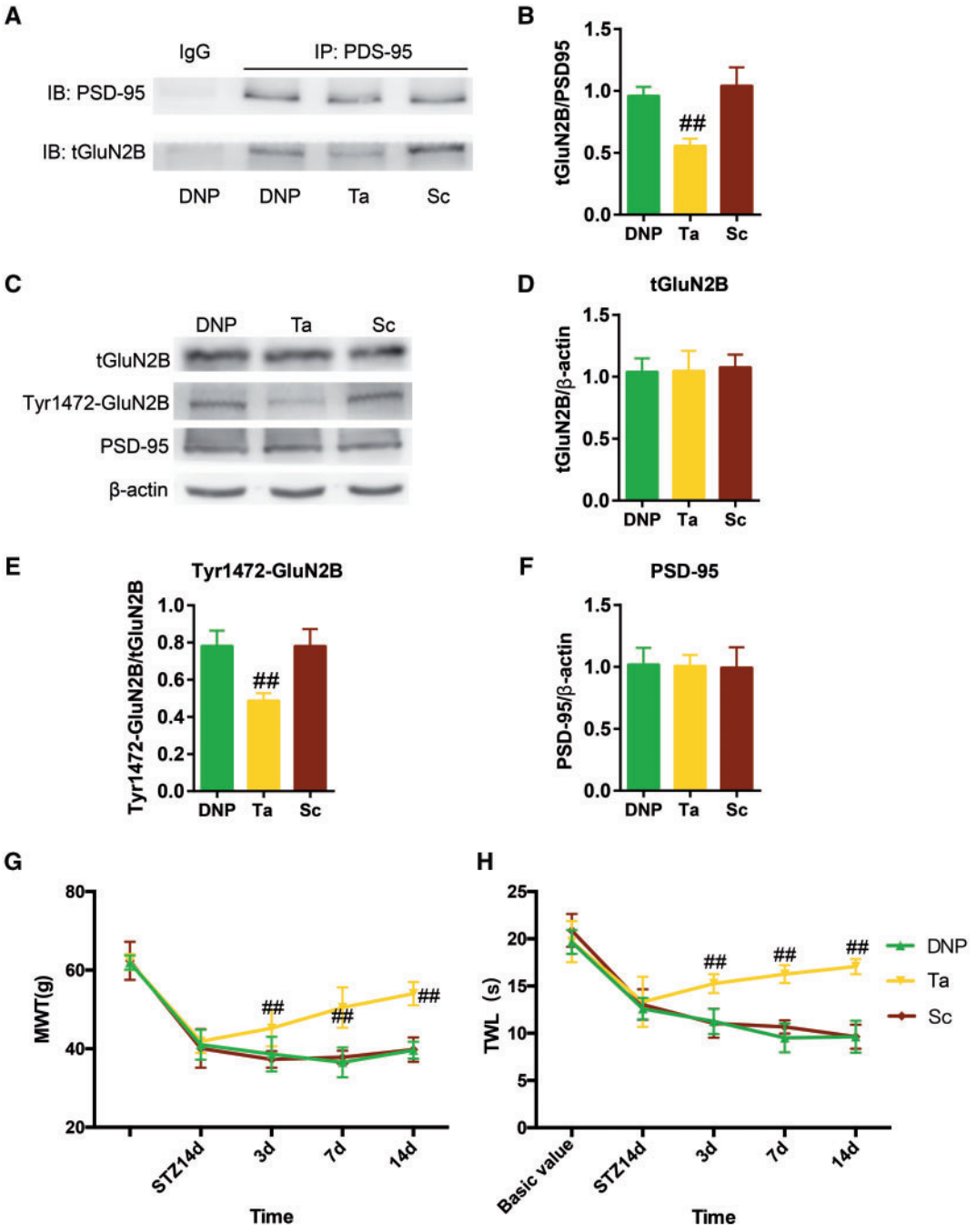

FIGURE 3. Effect of intrathecal Tat-NR2B9c on the spinal cord in GluN2B phosphorylation at Tyr1472 and on pain hypersensitivities in type-2 DNP rats. **(A)** Coimmunoprecipitation (Co-IP) of PSD-95 with tGluN2B in the 3 groups determined by Western blot. **(B)** Quantitative analysis of normalized optical density (tGluN2B/PSD-95) in the 3 groups. **(C)** Western blot results of the tGluN2B, Tyr1472-GluN2B, and PSD-95 protein in the 3 groups. **(D–F)** Histogram summarizes the integrated density values of tGluN2B, Tyr1472-GluN2B/tGluN2B, and PSD-95, respectively, in the 3 groups. **(G, H)** Changes in MWT **(F)** and TWL **(G)**. Group DNP: diabetic rats with neuropathic pain, Group Ta: DNP rats + Tat-NR2B9c, Group Sc: DNP rats + saline ($n = 6$ rats/each group). $^{\#\#}p < 0.05$ versus group DNP.

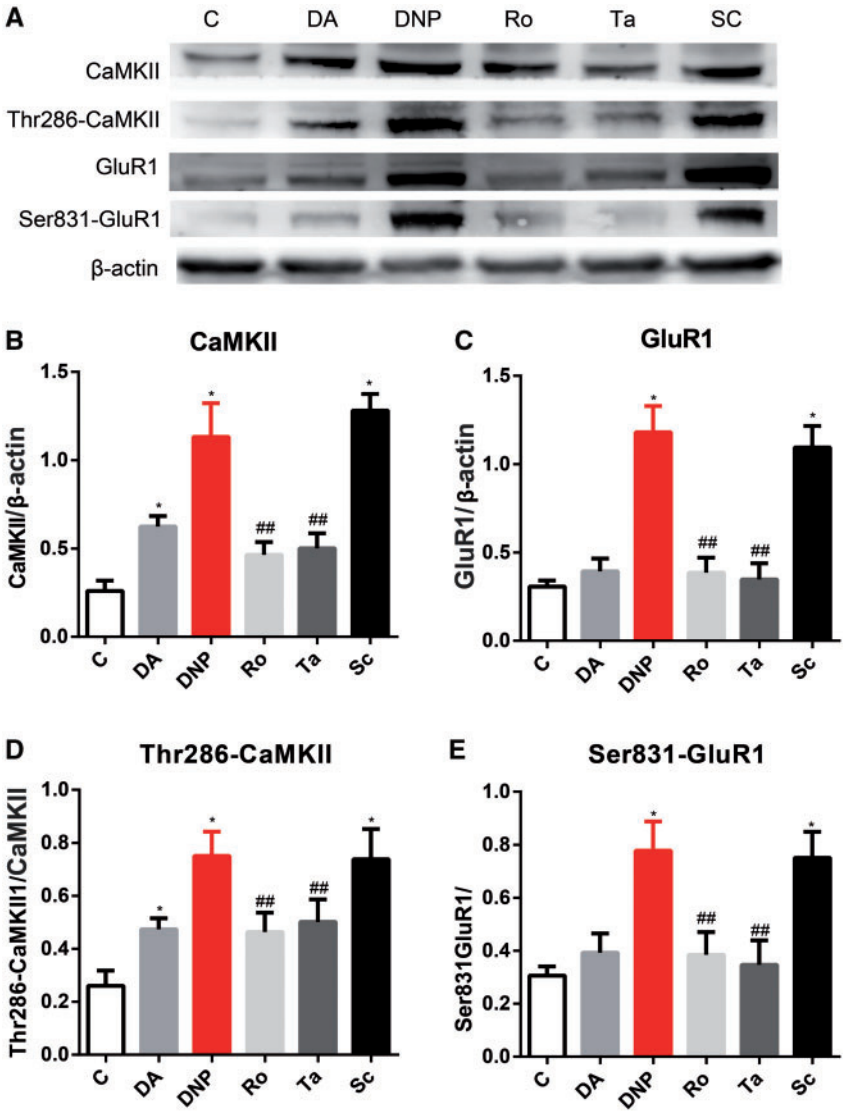

FIGURE 4. Expression of CaMKII, GluR1, and their phosphorylated counterparts in the spinal cord in the different groups. **(A)** Western blot results of the CaMKII, GluR1, Thr286-CaMKII, and Ser831-GluR1 protein in the different groups. **(B–E)** Histogram summarizes the integrated density values of CaMKII, GluR1, Thr286-CaMKII/CaMKII, and Ser831-GluR1/GluR1, respectively (normalized to the β-actin level), in the 6 groups ($n = 6$ rats/each group). *$p < 0.05$ versus group C, $^{\#\#}p < 0.05$ versus group DNP.

GluN2B may have participated in the development of type-2 DNP by activating the GluN2B subunit in the spinal cord.

The Increase in Expression of CaMKII, GluR1, and Their Phosphorylated Counterparts Was Dependent on the Activation of GluN2B in the Spinal Dorsal Horn of Type-2 DNP Rats

To explore the role of CaMKII and GluR1 in type-2 DNP, the changes in the expression of CaMKII, GluR1 and their phosphorylated counterparts in the spinal cord of type-2 DNP rats were examined. The amount of CaMKII and GluR1 increased in the spinal cord in group DNP (Fig. 4A–C; CaMKII: 1.13 ± 0.08, GluR1: 1.18 ± 0.06), when compared with group C (CaMKII: 0.26 ± 0.02, GluR1: 0.31 ± 0.01, $p < 0.05$) and group DA (CaMKII: 0.62 ± 0.02, GluR1: 0.39 ± 0.03, $p < 0.05$). The phosphorylation levels of CaMKII at Thr286 and GluR1 at Ser831 also increased in the spinal cord in group DNP (Fig. 4D, E; Thr286-CaMKII/CaMKII: 0.75 ± 0.04, Ser831-GluR1/GluR1: 0.78 ± 0.05), when compared with group C (Thr286-CaMKII/CaMKII: 0.26 ± 0.02, Ser831-GluR1/GluR1: 0.30 ± 0.01, $p < 0.05$) and group DA (Thr286-CaMKII/CaMKII: 0.47 ± 0.02, Ser831-GluR1/GluR1: 0.39 ± 0.03, $p < 0.05$). In order to further determine whether the activation of spinal GluN2B participated in this increase, the effects of intrathecal Ro25-6981 and Tat-NR2B9c on the increase in expression of CaMKII, GluR1, Thr286-CaMKII, and Ser831-GluR1 in the dorsal horn were analyzed by West-

ern blot. The results suggest that the intrathecal administration of either Ro25-6981, or Tat-NR2B9c blocked the increase in amount of CaMKII (Ro: 0.46 ± 0.03, Ta: 0.50 ± 0.03) and GluR1 (Ro: 0.39 ± 0.03, Ta: 0.35 ± 0.04), and the ratio of Thr286-CaMKII/CaMKII (Ro: 0.46 ± 0.03, Ta: 0.50 ± 0.03) and Ser831-GluR1/GluR1 (Ro: 0.39 ± 0.04, Ta: 0.35 ± 0.04) in the spinal dorsal horn of type-2 DNP rats ($p < 0.05$). These present findings show that the activation of CaMKII and GluR1 was dependent on the activation of GluN2B in the dorsal horn of type-2 DNP rats.

DISCUSSION

According to the International Diabetes Federation Diabetes Atlas, ∼415 million people worldwide have been diagnosed with diabetes most of whom had T2DM (2). Although both types-1 and -2 DM produce neuropathies with very similar symptoms, the fundamental mechanisms are essentially different (33). For example, type-1 DM patients may benefit from strict glucose control to prevent DN whereas that is not entirely the case for T2DM patients (35). The reasons why some patients with type-2 DN develop pain remain unknown.

T2DM-induced inflammation and peripheral nerve damage contribute to the NMDAR-mediated central sensitization of the spinal cord dorsal horn, which leads to the development and maintenance of DNP. Although NMDAR antagonists, such as ketamine, memantine, and MK-801, can effectively suppress the mechanical pain after spinal cord injury (16), these may also produce severe side-effects, including auditory and visual disturbances, hallucinations, feelings of unreality, dizziness, etc. These unwanted effects are correlated with the fact that NMDA receptors are not only involved in pathophysiological processes, such as chronic pain, but also participate in many important physiological processes (such as learning and memory) in CNS. Therefore, targeting the specific subunits (e.g. GluN2B) of NMDARs localized in nociceptive pathways may contribute to reducing the side effects (36). Furthermore, the level of GluN2B phosphorylation at Tyr1472 reflects the functional status of NMDARs and was essential for enhancing receptor function, as well as the maintenance of neuropathic pain induced by the transection of the L5 spinal nerve (23). To our knowledge, the mechanisms underlying type-2 DNP may differ from those of the neuropathic pain induced by spinal cord injury (7). For example, the expression of tGluN2B was elevated in the chronic constriction injury induced by neuropathic pain (37), but the expression of tGluN2B did not change (23). Therefore, it was necessary to detect both expression and phosphorylation of GluN2B in the present DNP model. We found that although the level of tGluN2B did not significantly change, the phosphorylation level of GluN2B at Tyr1472 significantly increased in the spinal cord of type-2 DNP rats. Furthermore, the selective antagonist of GluN2B by Ro25-6981 blocked the increase in Tyr1472-GluN2B in the spinal cord and attenuated the pain hypersensitivities in type-2 DNP rats. These results indicate that the phosphorylation of GluN2B in the spinal cord play an important role in the development and maintenance of type-2 DNP. No previous studies have reported the reagents that could ameliorate diabetes-related complications by reducing phosphorylation of GluN2B. Our results show that the GluN2B subunit may be a new molecular target for the therapy of type-2 DNP. However, further studies are needed to determine whether drugs that enhance the pain behaviors of DNP via increasing the phosphorylation of GluN2B.

Selective antagonists of GluN2B lead to the inhibition of several ion conductances, such as human ether-a-go-go related gene-mediated potassium currents, which may lead to serious cardiovascular complications (38). Therefore, we attempted to identify another strategy for producing analgesia with fewer side-effects. The PDZ-binding motif (tSXV) at the C-terminus of the NR2 subunits of NMDARs can bind the second PDZ domain of PSD-95. PSD-95 is a synaptic scaffolding protein that mediates the interaction of tyrosine kinase Fyn with GluN2B to promote Fyn kinase-mediated tyrosine phosphorylation of GluN2B (16). The administration of the mimetic peptide Tat-NR2B9c (which contains the specific C-tail of GluN2B to disturb the binding between PSD-95 and GluN2B) reduced the excitability of spinal neurons and formalin-induced pain behaviors (20). The present study revealed that the expression of spinal PSD-95 increased in type-2 DNP rats and that intrathecal injection of Tat-NR2B9c decreased the interaction of PSD-95 with GluN2B, reduced the GluN2B phosphorylation at Tyr1472 in the spinal cord, and rescued the decrease in MWT and TWL in type-2 DNP rats. However, this injection did not affect the level of spinal cord PSD-95. Our data suggest that the increase in PSD-95 was involved in type-2 DNP possibly through its coupling with GluN2B. Perturbing this coupling could decrease the phosphorylation of GluN2B in the spinal cord. Tat-NR2B9c reduced the T2DM-induced neuropathic pain possibly by perturbing the interaction of PSD-95-GluN2B, and subsequently decreasing the phosphorylation of GluN2B at Tyr1472 in the spinal cord.

We also found that the expression of CaMKII, GluR1, and their phosphorylated counterparts increased in the spinal cord of type-2 DNP rats. These increases were blocked after the intrathecal administration of either Ro25-6981, or Tat-NR2B9c. These results indicate that the expression of CaMKII, GluR1, and their phosphorylated counterparts were downstream of the GluN2B phosphorylation in the spinal cord and may play a key role in type-2 DNP.

In conclusion, this study demonstrated the key role of the spinal GluN2B/PSD-95-CaMKII-GluR1 signaling pathway in type-2 DNP. The intrathecal administration of Ro25-6981 or Tat-NR2B9c attenuated the pain hypersensitivities in type-2 DNP, without altering the acute or basal pain. Thus, targeting the interaction of GluN2B with PSD-95 may provide a novel therapeutic approach for type-2 DNP.

REFERENCES

1. Gonçalves NP, Vægter CB, Andersen H, et al. Schwann cell interactions with axons and microvessels in diabetic neuropathy. Nat Rev Neurol 2017;13:135–47
2. Sala D, Zorzano A. Differential control of muscle mass in type 1 and type 2 diabetes mellitus. Cell Mol Life Sci 2015;72:3803–17
3. Pop-Busui R, Lu J, Lopes N, et al. Prevalence of diabetic peripheral neuropathy and relation to glycemic control therapies at baseline in the BARI 2D cohort. J Peripher Nerv Syst 2009;14:1–13

4. Abbott CA, Malik RA, van Ross ER, et al. Prevalence and characteristics of painful diabetic neuropathy in a large community-based diabetic population in the U.K. Diabetes Care 2011;34:2220–4
5. Daousi C, MacFarlane IA, Woodward A, et al. Chronic painful peripheral neuropathy in an urban community: A controlled comparison of people with and without diabetes. Diabet Med 2004;21:976–82
6. Bouhassira D, Letanoux M, Hartemann A. Chronic pain with neuropathic characteristics in diabetic patients: A French cross-sectional study. PLoS One 2013;8:e74195
7. Zhou CH, Zhang MX, Zhou SS, et al. SIRT1 attenuates neuropathic pain by epigenetic regulation of mGluR1/5 expressions in type 2 diabetic rats. Pain 2017;158:130–9
8. Habib AA, Brannagan TH. Therapeutic strategies for diabetic neuropathy. Curr Neurol Neurosci Rep 2010;10:92–100
9. Spisák T, Pozsgay Z, Aranyi C, et al. Central sensitization-related changes of effective and functional connectivity in the rat inflammatory trigeminal pain model. Neuroscience 2017;344:133–47
10. Price DD, Mao J, Frenk H, et al. The N-methyl-D-aspartate receptor antagonist dextromethorphan selectively reduces temporal summation of second pain in man. Pain 1994;59:165–74
11. Traynelis SF, Wollmuth LP, McBain CJ, et al. Glutamate receptor ion channels: Structure, regulation, and function. Pharmacol Rev 2010;62:405–96
12. Aiyer R, Mehta N, Gungor S, et al. A systematic review of NMDA receptor antagonists for treatment of neuropathic pain in clinical practice. Clin J Pain 2018;34:450–67
13. Welters A, Kluppel C, Mrugala J, et al. NMDAR antagonists for the treatment of diabetes mellitus-Current status and future directions. Diabetes Obes Metab 2017;19:95–106
14. Boyce S, Wyatt A, Webb JK, et al. Selective NMDA NR2B antagonists induce antinociception without motor dysfunction: Correlation with restricted localisation of NR2B subunit in dorsal horn. Neuropharmacology 1999;38:611–23
15. Parsons CG. NMDA receptors as targets for drug action in neuropathic pain. Eur J Pharmacol 2001;429:71–8
16. Kim Y, Cho HY, Ahn YJ, et al. Effect of NMDA NR2B antagonist on neuropathic pain in two spinal cord injury models. Pain 2012;153:1022–9
17. Bai HP, Liu P, Wu YM, et al. Activation of spinal GABAB receptors normalizes N-methyl-D-aspartate receptor in diabetic neuropathy. J Neurol Sci 2014;341:68–72
18. Suo M, Wang P, Zhang M. Role of Fyn-mediated NMDA receptor function in prediabetic neuropathy in mice. J Neurophysiol 2016;116:448–55
19. Wang Z, Chen Z, Yang J, et al. Treatment of secondary brain injury by perturbing postsynaptic density protein-95-NMDA receptor interaction after intracerebral hemorrhage in rats. J Cereb Blood Flow Metab 2019;39:1588–601
20. D'Mello R, Marchand F, Pezet S, et al. Perturbing PSD-95 interactions with NR2B-subtype receptors attenuates spinal nociceptive plasticity and neuropathic pain. Mol Ther 2011;19:1780–92
21. Xu F, Zhao X, Liu L, et al. Perturbing NR2B-PSD-95 interaction relieves neuropathic pain by inactivating CaMKII-CREB signaling. Neuroreport 2017;28:856–63
22. Lin TB, Lai CY, Hsieh MC, et al. Neuropathic allodynia involves spinal neurexin-1$_\beta$-dependent neuroligin-1/postsynaptic density-95/NR2B cascade in rats. Anesthesiology 2015;123:909–26
23. Abe T, Matsumura S, Katano T, et al. Fyn kinase-mediated phosphorylation of NMDA receptor NR2B subunit at Tyr1472 is essential for maintenance of neuropathic pain. Eur J Neurosci 2005;22:1445–54
24. . Tavalin SJ, Colbran RJ. CaMKII-mediated phosphorylation of GluN2B regulates recombinant NMDA receptor currents in a chloride-dependent manner. Mol Cell Neurosci 2017;79:45–52
25. Lisman J, Schulman H, Cline H. The molecular basis of CaMKII function in synaptic and behavioural memory. Nat Rev Neurosci 2002;3:175–90
26. Zhou Z, Liang Y, Deng F, et al. Phosphorylated neuronal nitric oxide synthase in neuropathic pain in rats. Int J Clin Exp Pathol 2015;8:12748–56
27. Dang JK, Wu Y, Cao H, et al. Establishment of a rat model of type II diabetic neuropathic pain. Pain Med 2014;15:637.2– 46
28. Chen SR, Pan HL. Hypersensitivity of spinothalamic tract neurons associated with diabetic neuropathic pain in rats. J Neurophysiol 2002;87:2726–33
29. Lin Y, Sun Z. Current views on type 2 diabetes. J Endocrinol 2010;204:1–11
30. Brussee V, Guo G, Dong Y, et al. Distal degenerative sensory neuropathy in a long-term type 2 diabetes rat model. Diabetes 2008;57:1664–73
31. Muniyappa R, Lee S, Chen H, et al. Current approaches for assessing insulin sensitivity and resistance in vivo: Advantages, limitations, and appropriate usage. Am J Physiol Endocrinol Metab 2008;294:E15–26
32. Vrinten DH, Hamers FF. "CatWalk" automated quantitative gait analysis as a novel method to assess mechanical allodynia in the rat: A comparison with von Frey testing. Pain 2003;102:203–9
33. Chaplan SR, Bach FW, Pogrel JW, et al. Quantitative assessment of tactile allodynia in the rat paw. J Neurosci Methods 1994;53:55–63
34. Callaghan BC, Little AA, Feldman EL, et al. Enhanced glucose control for preventing and treating diabetic neuropathy. Cochrane Database Syst Rev 2012;CD007543
35. Callaghan BC, Hur J, Feldman EL. Diabetic neuropathy: One disease or two? Curr Opin Neurol 2012;25:536–41
36. Qu XX, Cai J, Li MJ, et al. Role of the spinal cord NR2B-containing NMDA receptors in the development of neuropathic pain. Exp Neurol 2009;215:298–307
37. Qian Y, Xia T, Cui Y, et al. The role of CaMKII in neuropathic pain and fear memory in chronic constriction injury in rats. Int J Neurosci 2019;129:146–54
38. Chizh BA, Headley PM. NMDA antagonists and neuropathic pain—Multiple drug targets and multiple uses. Curr Pharm Des 2005;11:2977–94